JOANNE: Joint dropsonde Observations of the Atmosphere in tropical North atlaNtic meso-scale Environments

Geet George[1], Bjorn Stevens[1], Sandrine Bony[2], Robert Pincus[3,4], Chris Fairall[4], Hauke Schulz[1],
Tobias Kölling[1], Quinn T. Kalen[5,★], Marcus Klingebiel[6,★], Heike Konow[7,★], Ashley Lundry[5,★],
Marc Prange[8,9,★], and Jule Radtke[8,9,★]

[1]Max Planck Institute for Meteorology, Hamburg, Germany
[2]LMD/IPSL, Sorbonne University, CNRS, Paris, France
[3]Cooperative Institute for Research in Environmental Sciences,
University of Colorado, Boulder, Colorado, USA
[4]NOAA Physical Sciences Laboratory, Boulder, Colorado, USA
[5]NOAA Aircraft Operation Center, Lakeland, Florida, USA
[6]Institute for Meteorology, University Leipzig, Leipzig, Germany
[7]Meteorological Institute, Universität Hamburg, Hamburg, Germany
[8]Meteorological Institute, Center for Earth System Research and Sustainability,
Universität Hamburg, Hamburg, Germany
[9]International Max Planck Research School on Earth System Modelling,
Max Planck Institute for Meteorology, Hamburg, Germany
★These authors contributed equally to this work.

Correspondence: Geet George (geet.george@mpimet.mpg.de)

Abstract. As part of the EUREC[4]A field campaign which took place over the tropical North Atlantic during January–February 2020, 1215 dropsondes from the HALO and WP-3D aircraft were deployed through 26 flights to characterize the thermodynamic and dynamic environment of clouds in the trade-wind regions. We present JOANNE (Joint dropsonde Observations of the Atmosphere in tropical North atlaNtic meso-scale Environments), the dataset that contains these dropsonde measurements and the products derived from them. Along with the raw measurement profiles and basic post-processing of pressure, temperature, relative humidity and horizontal winds, the dataset also includes a homogenized and gridded dataset with 10 m vertical spacing. The gridded data are used as a basis for deriving diagnostics of the area-averaged mesoscale circulation properties such as divergence, vorticity, vertical velocity and gradient terms, making use of sondes dropped at regular intervals along a circular flight path. A total of 85 such circles, ~ 222 km in diameter, were flown during EUREC[4]A. We describe the sampling strategy for dropsonde measurements during EUREC[4]A, the quality control for the data, the methods of estimation of additional products from the measurements and the different post-processed levels of the dataset. The dataset is publicly available (https://doi.org/10.25326/246, George et al., 2021b) as is the software used to create it (https://doi.org/10.5281/zenodo.4746312, George, 2021).

1   Introduction

> EUREKA! This is what I want to study for the rest of my life.

In an exclamation of serendipitous prescience Joanne Simpson is reported to have said these words upon learning about the possibility of studying trade-wind cumulus clouds through airborne measurements (Fleming, 2020). Her subsequent research proved foundational for tropical meteorology. Some 7 decades later, the 2020 ElUcidating the RolE of Cloud-Circulation Coupling in ClimAte (EUREC^{4}A) field campaign unwittingly expressed her exclamation of enthusiasm in finding purpose on the same topic.

The EUREC^{4}A field campaign took place in January–February 2020 and comprised measurements from many platforms. It adopted Barbados as its base of operations and focused its measurements in an area extending eastward of the Barbados Cloud Observatory (BCO; Stevens et al., 2016). EUREC^{4}A's initial scientific motivation, its subsequent evolution and the final execution are described in Bony et al. (2017) and Stevens et al. (2021). As these papers emphasize, a central element of EUREC^{4}A was the airborne release of dropsondes to characterize the mesoscale meteorological environment of cloud fields in the trades. The dropsondes were mostly deployed to enable accurate estimates of the mean vertical motion field, using an approach inspired by Lenschow et al. (1999, 2007) and adapted to dropsondes by Bony and Stevens (2019). Beyond estimating mesoscale vertical motion, the dropsondes were also aimed at characterizing the thermodynamic structure in this region. In the stratified atmosphere of the trades, the dropsondes can resolve strong vertical gradients in temperature and moisture over short vertical distances, which are difficult to measure through remote sensing (Stevens et al., 2017). The dropsondes are thus essential in characterizing the atmospheric environment within which many complementary measurements took place during EUREC^{4}A. The purpose of this paper is to describe the resultant dropsonde dataset, which we call the Joint dropsonde Observations of the Atmosphere in tropical North atlaNtic meso-scale Environments, or JOANNE, in honor of Joanne Simpson's seminal contributions to our field of research.

Recent instances of dropsonde datasets from tropical field campaigns include ones by Konow et al. (2019) in the north Atlantic summertime tropics and by Vömel et al. (2021) in the tropical east Pacific and Caribbean. Konow et al. (2019) published dropsonde data from the second phase of Next Generation Remote Sensing for Validation Studies (NARVAL2). They provide data on a uniform vertical grid at 30 m. JOANNE builds on this idea of a uniform vertical grid from Konow et al. (2019), albeit at 10 m spacing. We go further to provide derived quantities from the circle measurements as well as raw measurement files.

JOANNE comprises five levels of data products, with each successive level encompassing a greater degree of synthesis and post-processing. The basic measurements that go into the JOANNE data products, and how they were made, are discussed in Sect. 2. Quality control (QC) on the data is explained in Sect. 3, and evidence for a possible dry bias is presented in Sect. 4. The different levels of data products, and how they were constructed, are described in Sect. 5, and Sect. 7 concludes with a brief summary.

2   Sampling and measurements

2.1   Instrument and sensors

JOANNE is based entirely on data collected by Vaisala's RD-41 dropsondes (hereafter also "sondes"; Vaisala, 2020a). A dropsonde is similar to a radiosonde, with the exception that it is designed to be launched out of airborne platforms and sinks down through the atmosphere to the surface while making measurements. Each sonde has a cylindrical cardboard casing that houses within it the measurement sensors, a GPS receiver, a battery and a signal transmitter for communicating with the airborne receiving station. The casing is attached to a parachute that is designed to align the sonde properly for measurements and to reduce the fall speed.

The sondes carry three sensors – one each for measuring pressure (p), temperature (T) and relative humidity (RH), together referred to as the PTU sensors and with a sampling frequency of 2 Hz. The GPS receiver allows the position of the dropsonde to be tracked, from which ambient winds are estimated at a sampling frequency of 4 Hz. The sensors included in the sondes are the same as in Vaisala's RS-41 radiosondes (upsondes), which were also employed during EUREC^{4}A from the BCO and four other ship-based platforms (Stephan et al., 2021). Table 1 provides a brief summary of the type, the resolution and the expected performance from the sensors used in the RD-41 and RS-41 sondes.

2.2   Sonde deployment

A total of 1215 dropsondes were launched: 895 from the German High-Altitude Long Range aircraft (HALO) and 320 from the National Oceanic and Atmospheric Administration (NOAA) Lockheed WP-3D Orion N43-RF aircraft (P3). The P3 was operated as a part of the Atlantic Tradewind Ocean-Atmosphere Mesoscale Interaction Campaign (ATOMIC), which itself was a part of the EUREC^{4}A campaign. Throughout this paper, we use the term EUREC^{4}A to refer to both experiments. More details about HALO's and P3's participation in EUREC^{4}A are provided by Konow et al. (2021) and Pincus et al. (2021), respectively.

Both aircraft used the Airborne Vertical Atmospheric Profiling System (AVAPS; UCAR/NCAR, 1993) with eight simultaneous channels, for the operation of the dropsondes, as well as for the processing and quality control of collected

Table 1. Details about sensors used in the RD-41 and RS-41 sondes are provided. Repeatability is the standard deviation of differences in twin soundings. The values for the sensors are obtained from Vaisala (2020a), and values for wind measurements estimated from GPS are obtained from Vaisala (2020b). All numbers are provided in terms of absolute units, correspondingly in the first column.

Sensor/measurements (Units)	Type	Range	Least count	Repeatability
Pressure (hPa)	Silicon capacitor	Surface pressure to 3	0.01	0.4
Temperature (°C)	Platinum resistor	−90 to +60	0.01	0.1
Relative humidity (%)	Thin-film capacitor	0 to 100	0.1	2
Wind speed (m s^{-1})	Estimated from GPS	Max reported 180	0.1	0.15
Wind direction (°)	Estimated from GPS	0 to 360	0.1	2

Table 2. Total number of dropsondes launched, circles flown during the flight, and takeoff and landing times (in UTC, dates in yyyy-mm-dd) for the flight are provided with corresponding flight IDs. Numbers in parentheses in the second column indicate the number of good dropsondes per flight (explained in Sect. 3). Note that the table only shows circles with dropsonde launches. There were also circles flown with no dropsonde launches during EUREC[4]A.

Flight ID	Dropsondes (good)	Takeoff time	Landing time	Circles with dropsondes
P3-0117	23 (17)	2020-01-17 14:00:02	2020-01-17 20:50:00	1
P3-0119	28 (23)	2020-01-19 13:25:25	2020-01-19 21:47:51	1
P3-0123	38 (31)	2020-01-23 13:21:02	2020-01-23 21:29:14	2
P3-0124	16 (15)	2020-01-24 13:21:05	2020-01-24 22:14:32	0
P3-0131	25 (17)	2020-01-31 15:32:27	2020-01-31 23:36:04	1
P3-0203	22 (17)	2020-02-03 13:19:02	2020-02-03 19:21:57	1
P3-0204	31 (28)	2020-02-04 13:19:52	2020-02-04 21:54:08	1
P3-0205	29 (23)	2020-02-05 13:22:23	2020-02-05 21:59:43	1
P3-0209	32 (25)	2020-02-09 01:56:28	2020-02-09 10:13:37	2
P3-0210	32 (26)	2020-02-10 01:48:57	2020-02-10 09:54:42	2
P3-0211	44 (36)	2020-02-11 03:15:07	2020-02-11 11:21:50	2
HALO-0119	15 (12)	2020-01-19 09:34:25	2020-01-19 18:48:03	1
HALO-0122	73 (69)	2020-01-22 14:57:35	2020-01-23 00:10:30	6
HALO-0124	77 (71)	2020-01-24 09:29:30	2020-01-24 18:41:13	6
HALO-0126	75 (70)	2020-01-26 12:05:30	2020-01-26 21:20:49	6
HALO-0128	74 (71)	2020-01-28 14:58:34	2020-01-28 23:55:17	6
HALO-0130	4 (4)	2020-01-30 11:19:34	2020-01-30 15:08:20	0
HALO-0131	74 (68)	2020-01-31 15:08:35	2020-01-31 23:56:53	6
HALO-0202	89 (76)	2020-02-02 11:28:02	2020-02-02 20:13:24	6
HALO-0205	76 (65)	2020-02-05 09:15:51	2020-02-05 18:21:22	6
HALO-0207	73 (62)	2020-02-07 12:02:24	2020-02-07 21:11:40	6
HALO-0209	73 (66)	2020-02-09 09:14:31	2020-02-09 18:03:00	6
HALO-0211	61 (58)	2020-02-11 12:29:05	2020-02-11 21:37:29	5
HALO-0213	73 (69)	2020-02-13 07:56:10	2020-02-13 17:17:17	6
HALO-0215	51 (48)	2020-02-15 15:07:30	2020-02-16 00:12:44	5
HALO-0218	7 (1)	2020-02-18 10:11:05	2020-02-18 18:55:31	0

data. For HALO, the dropsondes are launched from a pneumatic chute controlled manually, which is located at the rear starboard side of the aircraft, slightly oriented towards the bottom of the fuselage. For the P3, the drop point is near the center of the fuselage, with a little offset to the starboard side. HALO typically launched sondes at an altitude between 10–10.5 km, whereas the P3 typically did so at ∼ 7.5 km. Some P3 sondes were launched at ∼ 3 km, when the P3 was flying typical lawn-mower patterns (straight, parallel, long legs connected by shorter, perpendicular legs; parts of some visible in the north in Fig. 1) at low altitudes to facilitate launching airborne expendable bathythermographs (AXBTs). The total number of dropsondes launched from the two aircraft per flight is given in Table 2.

Nearly 90 % (∼ 87 %) of the dropsondes launched reported data as expected, with partial data being recorded by a large percentage of remaining sondes. Only 51 (∼ 4 %) sondes provided no usable data. Almost all of these 51 sondes
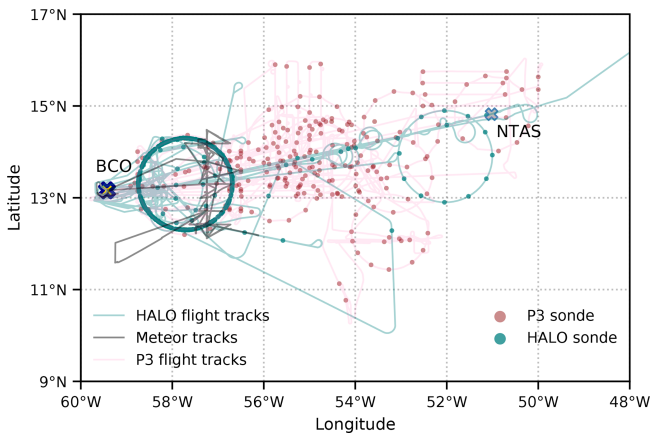
Figure 1. Map showing the launch locations of the dropsondes during EUREC[4]A from HALO (teal) and P3 (red). The flight paths for HALO (light teal), P3 (light pink) and Meteor (gray) are shown as shaded lines. The crosses near the west and east edges of the displayed domain mark the location of the BCO and the NTAS buoy, respectively.

failed because of an error in automatically detecting launch, the cause for which was later attributed to a manufacturing error in certain batches of dropsondes (Vaisala, personal communication). Success rates for the other aspects of measurements are described in more detail in Sect. 3.

A core part of the EUREC[4]A campaign was mesoscale circular flight patterns, which were adopted for most (1021 sondes, ∼ 84 %) of the dropsonde launches. The use of a repetitive flight pattern was based on a desire to provide consistent and comparable estimates of meteorological variables. Circles were chosen to facilitate estimates of the profile of the mesoscale (circle) divergence of the horizontal wind. Following the error analysis of Bony and Stevens (2019), each circle aimed to launch 12 sondes. The number of sondes launched per circle is provided in Table 3.

Most circles were flown along a fixed circular path, called the EUREC[4]A-circle (Stevens et al., 2021), which was planned with the center coordinates as 13.30° N, 57.72° W and a diameter of roughly 220 km. The location of the sonde launches shown in Fig. 1 highlights the density of HALO sondes concentrated along the circumference of the EUREC[4]A-circle. This circle was chosen such that complementary measurements are maximized between the aircraft and other platforms in EUREC[4]A. Measurements performed along the EUREC[4]A-circle were made irrespective of meteorological conditions and hence were unbiased. Flight times (see Table 2) were adjusted to best sample the diel cycle given operational constraints. HALO was mostly restricted to daylight hours, while the P3 made three flights at night and is the only sampling of the nighttime trades from EUREC[4]A dropsondes.

The actual mean diameter of all EUREC[4]A-circles marked by dropsonde launches was 222.82 km, and the mean center

was 13.31° N, 57.67° W. One circuit around the EUREC[4]A-circle took HALO roughly 60 min to execute at a flight level of about 9.5 km, resulting in sonde launches separated by about 5 min. There were 85 dropsonde circles flown during EUREC[4]A (see details in Table 3), and 73 of these were EUREC[4]A-circles, with HALO flying 70 of them and the rest flown by the P3. Of the 12 circles flown which were not EUREC[4]A-circles, one (HALO-0215_c3) was flown by HALO to provide spatial contrast for comparison with measurements in the EUREC[4]A-circle. The remaining 11 non-EUREC[4]A circles were flown by the P3 and were mostly centered on the location of the NOAA research vessel *Ronald H. Brown*. The flight track of some of the P3 circles was approximated by a dodecagon.

Sondes were also dropped to sample conditions upwind and in the vicinity of EUREC[4]A-circles, to aid calibration of other instruments, as references for satellite underpasses, and to support surface-based measurements from research vessels and buoys. For instance, HALO typically separated a set of three standard EUREC[4]A-circles by an upwind "excursion" toward the Northwest Tropical Atlantic Station buoy (NTAS) near 14.82° N, 51.02° W, along which one to three sondes were launched per flight.

Additional details and strategies for HALO and P3 flights which may be informative for those sondes not launched on standard circles can be found in Konow et al. (2021) and Pincus et al. (2021), respectively.

The maximum drift of the sondes from their launch locations in the horizontal space had a median of around 2.5 km, as seen in Figs. 2 and 3. In the lower troposphere, the drift was generally more along the zonal direction than in the meridional direction, with sondes tending to drift towards the southeast of the launch location. Due to a climatological wind reversal near 3 km, the maximum displacement for HALO is at about this level, whereas for the P3 which dropped its sondes from a lower altitude and thus sampled less of the upper level westerlies, the maximum displacement is at the surface. This also explains why the drift of the P3 sondes is systematically to the west of the drop and less directionally biased for the HALO sondes. The P3 sondes typically sampled the sub-cloud layer ∼ 0.03° southwest of the launch location, whereas for HALO sondes, the direction of drift was influenced strongly by the winds above 3 km and therefore varied between different flight days.

2.3   Raw data and initial processing

The raw data collected on the aircraft by AVAPS and the subsequent processing with the Atmospheric Sounding Processing Environment (ASPEN; Martin and Suhr, 2021) software constitute Levels 0 and 1 of JOANNE, respectively. The data included as part of these two levels involve no external adjustments other than the standard processing and quality control by AVAPS and ASPEN – both state-of-the-art tools for dropsonde measurements.

Table 3. Details of circles flown during EUREC[4]A. Circle time (in UTC) is the mean launch time for all sondes in the circle. Longitude (° E), latitude (° N) and diameter (km) are those associated with the center of a least-squares fitted circle to all sondes. Dropsondes show the total number of sondes launched in each circle. The numbers in parentheses (L4) show the number of good sondes (explained in Sect. 3) used for regression in Level 4.

Circle ID	Circle time	Longitude	Latitude	Diameter	Dropsondes (L4)
P3-0117_ci1	15:55	−51.00	14.84	181.86	12 (9)
P3-0119_ci1	15:02	−52.97	14.50	180.90	12 (9)
P3-0123_ci1	14:31	−54.96	14.38	186.96	12 (11)
P3-0123_ci2	20:12	−55.68	13.29	185.34	12 (9)
P3-0131_ci1	16:53	−54.38	13.84	184.74	12 (7)
P3-0203_ci1	14:40	−54.50	13.92	183.19	13 (11)
P3-0204_ci1	14:50	−53.14	13.49	184.45	12 (11)
P3-0205_ci1	15:12	−53.26	12.23	179.63	12 (10)
P3-0209_ci1	04:55	−57.67	13.26	243.92	12 (10)
P3-0209_ci2	06:22	−54.87	13.84	187.64	12 (10)
P3-0210_ci1	04:55	−57.74	13.30	220.41	12 (7)
P3-0210_ci2	06:12	−54.78	13.77	184.77	12 (11)
P3-0211_ci1	06:06	−57.71	13.30	221.59	12 (12)
P3-0211_ci2	07:16	−55.49	14.23	185.69	13 (10)
HALO-0119_c1	17:53	−57.86	13.27	186.65	12 (10)
HALO-0122_c1	15:45	−57.70	13.27	222.45	12 (12)
HALO-0122_c2	16:58	−57.71	13.28	223.80	12 (12)
HALO-0122_c3	18:09	−57.72	13.27	220.95	12 (11)
HALO-0122_c4	20:12	−57.70	13.29	224.13	13 (12)
HALO-0122_c5	21:27	−57.71	13.29	223.64	12 (11)
HALO-0122_c6	22:34	−57.71	13.31	225.99	12 (11)
HALO-0124_c1	10:19	−57.62	13.23	231.01	13 (10)
HALO-0124_c2	11:30	−57.66	13.28	224.16	13 (13)
HALO-0124_c3	12:42	−57.69	13.28	223.83	12 (12)
HALO-0124_c4	13:57	−57.68	13.27	223.80	12 (12)
HALO-0124_c5	15:07	−57.69	13.27	223.98	12 (12)
HALO-0124_c6	16:16	−57.68	13.27	223.47	13 (11)
HALO-0126_c1	12:49	−57.68	13.29	224.27	12 (12)
HALO-0126_c2	14:01	−57.67	13.30	219.53	12 (10)
HALO-0126_c3	15:10	−57.69	13.28	221.75	12 (11)
HALO-0126_c4	17:47	−57.67	13.29	224.49	12 (12)
HALO-0126_c5	19:00	−57.69	13.28	221.71	12 (11)
HALO-0126_c6	20:19	−57.67	13.29	224.16	12 (12)
HALO-0128_c1	15:46	−57.70	13.30	223.86	12 (12)
HALO-0128_c2	16:57	−57.70	13.30	223.84	12 (12)
HALO-0128_c3	18:11	−57.69	13.32	221.09	12 (11)
HALO-0128_c4	20:25	−57.71	13.32	226.18	12 (11)
HALO-0128_c5	21:41	−57.70	13.30	223.89	12 (12)
HALO-0128_c6	22:55	−57.70	13.30	224.00	13 (12)
HALO-0131_c1	15:57	−57.70	13.31	225.87	11 (11)
HALO-0131_c2	17:06	−57.72	13.31	226.37	12 (11)
HALO-0131_c3	18:20	−57.69	13.30	219.07	12 (10)
HALO-0131_c4	20:28	−57.69	13.29	224.03	12 (12)
HALO-0131_c5	21:42	−57.70	13.29	224.15	12 (12)
HALO-0131_c6	22:54	−57.68	13.29	221.11	12 (11)
HALO-0202_c1	12:12	−57.72	13.29	224.80	12 (10)
HALO-0202_c2	13:18	−57.71	13.28	223.70	12 (11)
HALO-0202_c3	14:27	−57.71	13.27	225.77	13 (11)
HALO-0202_c4	16:55	−57.70	13.28	226.26	12 (9)
HALO-0202_c5	18:03	−57.72	13.28	222.28	12 (11)
HALO-0202_c6	19:06	−57.71	13.29	224.82	13 (12)
HALO-0205_c1	09:59	−57.70	13.29	220.90	12 (11)

Table 3. Continued.

Circle ID	Circle time	Longitude	Latitude	Diameter	Dropsondes (L4)
HALO-0205_c2	11:11	−57.70	13.28	220.83	14 (11)
HALO-0205_c3	12:21	−57.72	13.26	223.22	12 (11)
HALO-0205_c4	15:03	−57.71	13.23	224.79	12 (10)
HALO-0205_c5	16:11	−57.73	13.28	226.25	13 (10)
HALO-0205_c6	17:24	−57.73	13.26	221.54	12 (11)
HALO-0207_c1	12:47	−57.73	13.28	223.83	12 (12)
HALO-0207_c2	13:57	−57.74	13.28	223.89	12 (11)
HALO-0207_c3	15:08	−57.73	13.29	223.34	12 (7)
HALO-0207_c4	17:44	−57.74	13.28	228.51	12 (10)
HALO-0207_c5	18:57	−57.73	13.28	224.13	12 (12)
HALO-0207_c6	20:14	−57.75	13.30	226.98	12 (9)
HALO-0209_c1	10:00	−57.70	13.26	224.99	12 (11)
HALO-0209_c2	11:12	−57.70	13.26	224.47	12 (10)
HALO-0209_c3	12:26	−57.68	13.28	221.13	12 (11)
HALO-0209_c4	14:27	−57.70	13.26	224.30	12 (11)
HALO-0209_c5	15:37	−57.70	13.26	223.40	12 (11)
HALO-0209_c6	16:53	−57.68	13.28	220.94	12 (11)
HALO-0211_c1	13:25	−57.71	13.32	229.02	12 (10)
HALO-0211_c2	14:38	−57.66	13.30	223.89	12 (12)
HALO-0211_c3	15:49	−57.64	13.31	221.66	11 (11)
HALO-0211_c4	17:05	−57.67	13.32	225.76	12 (11)
HALO-0211_c5	18:25	−57.66	13.30	224.00	12 (12)
HALO-0213_c1	08:43	−57.65	13.32	223.47	12 (12)
HALO-0213_c2	09:55	−57.65	13.33	222.41	12 (10)
HALO-0213_c3	11:04	−57.65	13.32	223.76	12 (12)
HALO-0213_c4	13:33	−57.65	13.32	223.49	12 (12)
HALO-0213_c5	14:49	−57.65	13.32	223.42	12 (12)
HALO-0213_c6	16:03	−57.66	13.32	224.27	12 (11)
HALO-0215_c1	16:06	−57.73	13.29	223.31	11 (11)
HALO-0215_c2	17:14	−57.68	13.25	229.76	8 (7)
HALO-0215_c3	18:47	−52.04	13.91	224.94	12 (11)
HALO-0215_c5	22:10	−57.67	13.33	222.44	13 (13)
HALO-0215_c6	23:12	−57.59	13.22	237.56	7 (6)

2.3.1 Level 0 (raw data)

Level 0 includes the raw files generated by AVAPS during dropsonde measurements. For every dropsonde launch, multiple files are generated, which store the collected data in different formats, with there being some extent of information overlap between them. These files have names starting with a capitalized letter and are described in Table 4 with the corresponding letter as the file type.

In addition to these files, information about the hardware and the aircraft data is generated and stored each time the AVAPS system is switched on, usually once per flight. These files have names preceded by a number, and the type and content of these files are given in Table 4.

All Level-0 files of a single day (as per UTC) are stored in their respective date directories, with their names in the format YYYYMMDD. The P3 and HALO directories are separated into two different directories named after the respective aircraft.

2.3.2 Level 1 (ASPEN processed data)

Level 1 includes all files from Level 0 after processing by ASPEN. ASPEN takes in D-type files (see Table 4) as input and gives an output of quality controlled files. For JOANNE, the D files were supplied as input to BatchASPEN v3.4.3, and all output files have the suffix _QC. The files are in NetCDF format. For ASPEN processing, we used the standard *editsonde* configuration. A detailed explanation of the file-structure of these _QC.nc files and the processing steps carried out by ASPEN are outlined in detail by Martin and Suhr (2021). These Level-1 _QC.nc files serve as the input for further processing in JOANNE.

3 Quality control (QC)

For the data products post Level 1, JOANNE aims to provide sounding profiles that do not contain any obvious measurement errors and contain minimal missing data records. Af-
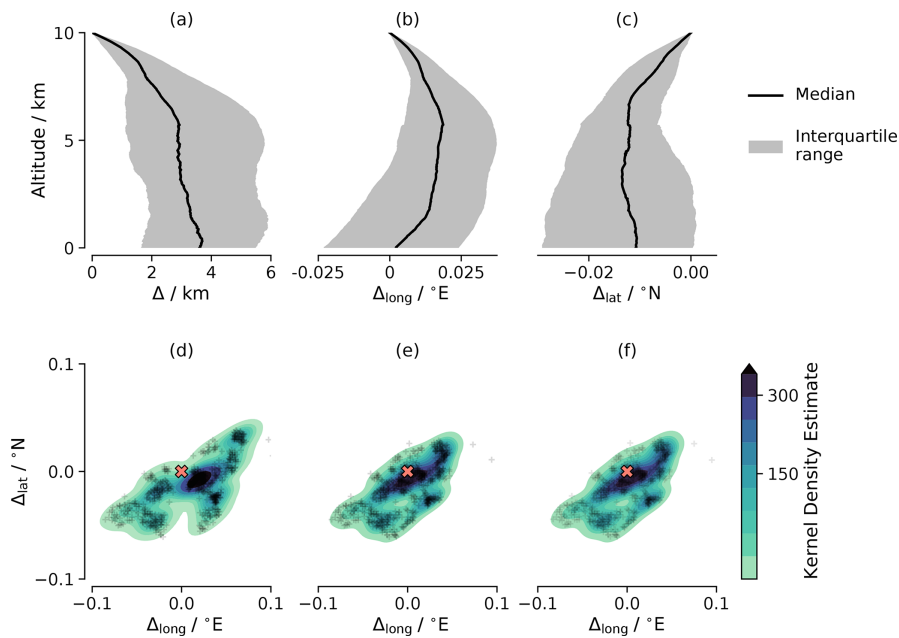
Figure 2. An overview of the drift in HALO sondes. Δ indicates horizontal displacement in sondes from launch location. Panels **(a)**–**(c)** show the median drift from launch and the corresponding interquartile range for **(a)** horizontal displacement, **(b)** longitude and **(c)** latitude. Panels **(d)**–**(f)** show as colors the kernel density estimates (KDEs) of drift from launch location (red cross) at **(d)** median altitude of maximum drift in the profile, $\tilde{z} = 3140\,\text{m}$, **(e)** at sub-cloud layer mean (0–500 m) and **(f)** at an altitude of 2 km, where the cloud-top layer is usually present.
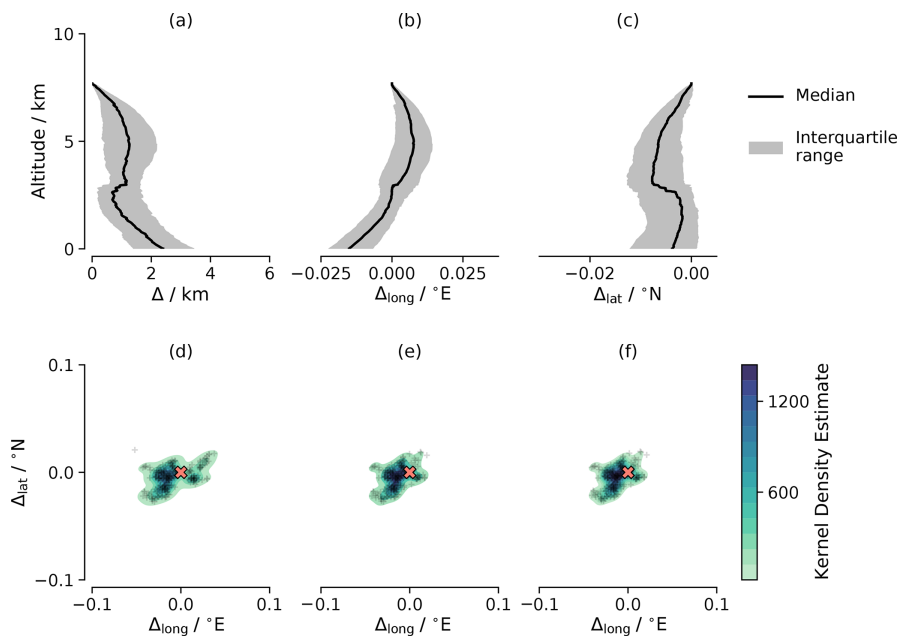
Figure 3. Same as Fig. 2, but for P3 sondes instead of HALO sondes. For **(d)**, median altitude of maximum drift in the profile, $\tilde{z} = 10\,\text{m}$.

ter the ASPEN processing, we run additional QC tests on all Level-1 sounding profiles and filter out soundings that do not meet these objectives. Profiles which are filtered out during this QC are not included in Level 2 and onwards. We believe that soundings passing such a QC stage would best fulfill the purpose of the dropsondes – to characterize the EUREC[4]A atmospheric environment – with little to no troubleshooting at the user end. However, users who wish to pursue a specific measurement that did not make it past the QC stage can still find it in the exhaustive Level-0 and Level-1 data products.

Table 4. File types included in Level 0, which are all files in the raw data collected by the dropsondes, and a brief description of what they entail.

File type	Description
A files	Sounding attribute file; includes channel configuration, COM port data, hardware configuration, launch obs data, sensor errors, aircraft data, software config and firmware information
B files	File containing binary data; same as D files
C files	Sounding data stored as comma-separated-value files
D files	Raw sounding data recorded for timestamp at every 0.25 s
D_P files	Only post-launch raw data; same as D files
R files	Receiver port data: signal strength and receiver frequency
0_SysLog files	Comma-separated-value file of all AVAPS system logs
1_Aircraft files	TXT file of aircraft position data in the IWGADTS format (IWG1)
2_GPSRef files	TXT file of GPS data: GPGGA (system fix data) and GPRMC (minimum specific GPS/Transit data)
3_SpecAnlyzr files	TXT file of logs of spectral analyzer

A sounding's success in the QC stage is provided by a parameter *qc_flag*, which has possible values of *good*, *bad* and *ugly*. The values stand for fully usable, non-usable and partially usable data, respectively, and are described in more detail later with relevant context. Only soundings flagged as good are included in JOANNE after Level 1. A sounding's qc_flag value is determined by its collective performance in three tests that are designed with the aforementioned QC objectives in mind. These tests are listed as follows.

1. *Launch detection test (ld_test).* This test filters sondes that failed to detect an automatic launch.

2. *Profile fullness test (sat_test).* This test filters sondes that did not record measurements for at least 80 % of the time measured in the profile.

3. *Low-altitude measurements test (low_test).* This test filters sondes whose measurements in the lower levels of the atmosphere do not fall within the expected bounds of parameter values.

The details of how a sounding's performance is judged with these tests and how these tests combine to give the qc_flag value for the sounding are explained further in this section.

3.1 Launch detection test (ld_test)

This test checks whether the sonde detected a launch automatically. If a sonde fails to automatically detect a launch, it does not switch to high-power signal transmission and thus fails to send data back to the AVAPS PC in the aircraft after it has passed further than a short range. The receiver in the aircraft usually failed to detect any signal from such sondes after they had fallen below pressure levels of 300 hPa.

The primary method to check launch detection is to parse through the sounding attribute log files (A type; see Table 4) in Level 0. These files have names starting with "A" and are followed by the date and time of launch. The file extension is the number of the channel used to initialize the sonde and receive its signal. Note that for sondes that did not detect a launch, the file name has time when the sonde was initialized, whereas for the rest, the file name is for the time of the detected launch. The log file contains an internal record termed "Launch Obs Done?". If this value is 1, the launch was detected; if it is 0, launch was not detected. A sounding's success in this test is marked by the parameter ld_test and takes values of good or bad, if the corresponding sondes have a successful launch detection or a failed launch detection, respectively. For six sondes, A files were found to be missing in the raw data. These sondes have been tagged as ugly for the ld_test.

3.2 Profile fullness test (sat_test)

This test checks the abundance of measurements within a sounding profile relative to the flight time of the sonde. For a raw measurement profile, time is the independent dimension along which records of measurements are made. The time record is given by the 4 Hz GPS measurements, which means that for the 2 Hz PTU measurements every other record is a missing value. Ideally, all parameters (except u, v) will have measurements at every other time record and u, v at every time record, but in practice, the number of records with measurements always falls short of the ideal number. This is because the time records also include values during initialization as well as during a little before and after the launch, when no signal can be sent back to the AVAPS PC. Thus, the
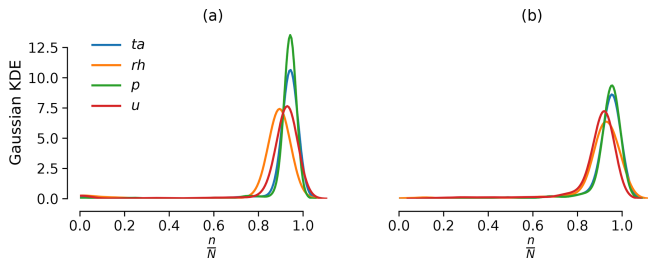
Figure 4. Kernel density estimate of ratio of actual measurement counts (n) out of maximum possible count of measurements (N), based on the timestamp records in each Level-1 sonde file for **(a)** HALO and **(b)** P3. For u, N would be the total timestamp records in any given sonde profile, whereas for the rest it would be half that. In the legend, labels stand for temperature (ta), relative humidity (RH), pressure (p) and eastward wind (u). The northward wind (v) has the same distribution as u and is hence not shown.

ratio of actual measurements to total possible measurements is lower than the ideal estimate of 1.

The profile fullness test is run by checking the abundance of measurements individually for all parameters in a sounding. The success of the test for a parameter ϕ is recorded in a corresponding parameter ϕ_test, e.g., p_test corresponding to p (pressure), and this success is determined by the ratio of the count of its measurements (n) to its total possible measurements (N), denoted by

$$\phi_{\mathrm{sat}} = \frac{n(\phi)}{N(\phi)}. \tag{1}$$

Accounting for the different sampling rates of the GPS and PTU measurements, the distributions of ϕ_{sat} are shown in Fig. 4, which shows that peaks start to flatten below 0.8. Thus, we set a threshold value of 0.8, and if parameter ϕ has ϕ_{sat} lower than this threshold, then it is taken as not having a complete profile, and ϕ_test is flagged as ugly. If ϕ_{sat} exceeds or matches the threshold, ϕ_test is flagged as good. If all values are missing, i.e., $\phi_{\mathrm{sat}} = 0$, then ϕ_test is flagged as bad.

Whereas the aforementioned tests (ϕ_test) recorded the success for every parameter in a sounding, we use sat_test to record the success of a sounding. For a given sounding, if all parameter tests are good, the sounding's sat_test is flagged as good. Similarly, if all individual parameter tests are bad, sat_test is flagged as bad. If neither of these conditions is met, sat_test is flagged as ugly.

Figure 4 shows that the abundance of RH values compared to those of pressure (p) and temperature (T) is lower. This is because the RH sensor takes longer to equilibrate to ambient conditions when compared with the other two. This results in fewer measurement records for RH than p and T for the same number of timestamps in the profile.

For HALO's RH measurements, there were more failures in ASPEN's *Filter Check* and *Final Smoothing*, compared to those for p and T. These checks are part of the post-

processing algorithm of ASPEN. The former removes suspect data that deviate by a certain value after the data series is passed through a low-pass filter. As per the standard editsonde configuration that we use, the deviation and the filter wavelength used are 20 % and 20 s, respectively. For the final smoothing, all data (p, T, RH and winds) undergo bspline smoothing with a wavelength of 10 s (Martin and Suhr, 2021).

3.3 Low-altitude measurement test (low_test)

This test functions as a sanity check for the measurements from a sounding in the lower levels of the atmosphere, which is mostly near the surface except for one test where the check is for the lowest 4 km. Similar to the profile fullness test, this test is also determined by the success of parameters over different individual tests. The success of these individual tests is recorded with a parameter name same as that of the corresponding test name. For each of these tests, if the sounding passes the test, it is marked as good, otherwise as bad. The individual tests and their criteria for passing are as follows.

1. *low_p_test*

    This test checks if maximum pressure measured in a sounding is within bounds (1000–1020 hPa), and if so, the sounding passes the test. If the maximum value of p is greater than the upper bound, it is unrealistic, and if it is lesser than the lower bound, it means that the sonde did not measure the near-surface levels of the atmosphere. This test does not check any GPS values. Even if there were no pressure measurements higher than 1000 hPa, there may still be GPS measurements in the low-altitude levels. Such sondes can still be useful for wind and wind-derived products.

2. *low_t_test*

    This test checks if air temperature measured in a sounding is within bounds. It sets two criteria for bounds: (a) maximum air temperature recorded should not be greater than 30 °C, and (b) mean T in the bottom 100 m should not be lesser than 20 °C. If either of the above limits is violated, measurement of T for the sounding is considered out of bounds and marked as bad. The sonde is also marked bad, if there are no measurements in the bottom 100 m (by GPS altitude (*gpsalt*) in Level 1).

3. *low_rh_test*

    This test checks if relative humidity measured in a sounding is within bounds. The criterion is that mean RH in the bottom 100 m should not be less than 50 %. If this bound is violated, RH for the sonde is considered out of bounds and marked as bad. The sonde is also marked bad if there are no measurements in the bottom 100 m.

Table 5. Determination of qc_flag value based on success of sounding in the three QC tests – ld_test, sat_test and low_test. The asterisk indicates that any value for the test satisfies the condition.

ld_test	sat_test	low_test	qc_flag
Good	Good	Good	Good
Bad	*	*	Bad
	Bad	Bad	Bad
All other combinations			Ugly

Table 6. Count of sondes that passed each QC test, separated by platforms.

Platform	Classification	ld_test	sat_test	low_test	qc_flag
HALO	Good	854	814	831	810
	Bad	41	1	40	41
	Ugly	0	80	24	44
P3	Good	310	269	280	263
	Bad	4	0	8	4
	Ugly	6	51	32	53

4. *low_z_test*

   This test checks if minimum *gpsalt* of a sounding is within bounds, i.e., ≤ 30 m above mean sea level. A value higher than the bound means there are no near-surface measurement values of GPS and consequently horizontal winds. This flag does not include any geopotential height values. Even if there are no GPS values below 30 m, there may still be PTU measurements in the lowest levels.

5. *palt_gpsalt_rms_test*

   This test checks if the root mean square (rms) difference between geopotential altitude (palt) and the GPS altitude (gpsalt), for values below 4 km, is lower than 100 m. If the estimated rms difference is below the limit, then the sounding is flagged as good. If the estimated rms difference is greater than the limit, or if there are no values of either *palt* or *gpsalt* overlapping in the lower 4 km, then the sounding is flagged as bad. The lack of overlap could be because there are either no palt values or no gpsalt values, or both.

Based on the success in the aforementioned individual tests, the overall success of a sounding for the low-altitude measurement test is recorded in the parameter low_test. If all individual tests are flagged as good, the low_test is flagged as good, and similarly, if all individual tests are flagged as bad, the low_test is flagged as bad. If neither of these conditions is met, the sounding's low_test is flagged as ugly.

Note that the bounds used for the individual tests are all considered keeping in mind the EUREC⁴A region and conditions. For a similar QC in a different region or environment, the bounds for the parameters will likely be different.

3.4 *qc_flag*

The overall success of a sounding is recorded as values of good, bad or ugly in the qc_flag parameter and is determined by the combination of success through the three QC tests, as shown in Table 5.

Table 6 summarizes the statistics of the QC tests for HALO and P3. Although the process of classifying the sondes can be simplified by other combinations of the sat_test and low_test values, the method we present ensures no good

sondes are omitted, and no bad sondes are admitted. The rest of the sondes, the ugly sondes, still have data that can be salvaged and, after some additional QC, can be combined with the other good sondes depending on the user's objective.

JOANNE provides a status file per platform, which stores the results for each individual test and group of tests mentioned above, as well as the final qc_flag classification for each sounding. Thus, the user can still mold the classification based on their objectives and add or remove tests to the process and customize the sonde selection for themselves.

4 Dry bias in HALO dropsondes

The radiosonde measurements during EUREC⁴A taken from the BCO and the research vessel *Meteor* show evidence of a dry bias in the humidity measurements of the HALO dropsondes. The HALO measurements are bounded by *Meteor*'s on the upwind side and BCO's on the downwind side (see Fig. 1). Since all three platforms have unbiased sampling, we expect that the HALO distribution should be between the other two. Figure 5 shows that the BCO and *Meteor* distributions of RH align closely throughout the lower troposphere, and thus HALO measurements should not differ. The offset in the HALO measurements towards lower RH values suggests a dry bias in the HALO sondes. Since the sensors for the dropsondes and the radiosondes are the same, an instrument difference can be ruled out. Further comparisons with other water vapor measurements in the vicinity such as the radiosondes from the ship *Ron Brown*, surface humidity measurements from both ships and dropsondes from the P3 aircraft also show HALO's median specific humidity to be lower than expected (not shown).

A possible contamination of the polymer film in the moisture sensor could affect its dielectric constant, whose fluctuations with respect to relative humidity are subsequently affected. The most plausible explanation is the lack of reconditioning for HALO dropsondes, which resulted in some trace gas pollutants being retained on the humidity sensor and should otherwise have been removed during the reconditioning. The P3 sondes were reconditioned before data collection, and the protocols for P3 and HALO therefore differed in this aspect. This leads us to believe that the dry bias
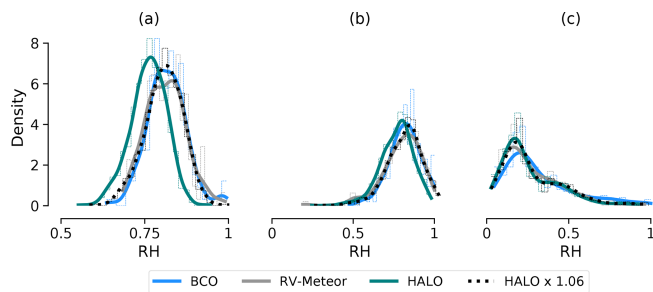
Earth Syst. Sci. Data, 13, 5253–5272, 2021

https://doi.org/10.5194/essd-13-5253-2021

Figure 5. Spread (kernel density estimates) in relative humidity values from soundings made by BCO, *Meteor* and HALO at a **(a)** mean of 0–500 m, **(b)** mean of 750–1500 m and **(c)** mean of 2000–4000 m. The last item in the legend is for RH values of HALO multiplied by 1.06. To coincide with HALO measurement times, BCO and *Meteor* soundings between 03:00 and 09:00 UTC have been excluded from these distributions, which has a relatively insignificant impact.

is observed only in HALO dropsondes because of the absent reconditioning. In the case of radiosondes, the reconditioning is part of the automatic calibration process, and so it is not expected to cause problems.

A multiplicative correction factor of 1.06 to the RH values (dotted line in Fig. 5) aligns the HALO distributions well with the BCO and *Meteor* distributions. The success of this simple rescaling, in matching both the mean and the variance of the distributions, suggests that the bias is both multiplicative and systematic. Had the bias come from a subset of the sondes, a multiplicative correction to match the mean would have resulted in a broader distribution. Had the bias been an additive one, then the correction would have not been as successful at all heights. It is not, however, understood how the contamination of the sensor leads to this dry bias and why the multiplicative correction appears to work so well. However, given the information we have, the multiplicative correction is the best option to correct for the dry bias. Therefore, products from Level 2 onwards include this correction. The values in the `rh` variable only for the HALO sondes are therefore multiplied by 1.06 when including them in Level 1 from Level 2. All subsequent products in Levels 3 and 4, therefore, have variables derived from the corrected moisture.

Users of the data may note that the correction in HALO dropsonde measurements will propagate into other variables, such as precipitable water (PW), pressure velocity and moisture gradients (since it is apparently multiplicative) and will even have a slight effect on estimates of geopotential altitude which depend on the atmospheric density and hence moisture content. Should the user wish to use the uncorrected moisture values, they can be accessed in Levels 0 and 1.

5 Data products

5.1 Level 2 (quality-controlled sounding data)

The Level-2 NetCDF files contain data from individual soundings, which passed with a qc_flag value of good from the QC stage (discussed in Sect. 3). For Level 2, only variables that are measurements from the dropsonde sensors are included. Redundant state variables are not carried forward from the Level-1 files. Products up to Level 2 maintain the raw measurement profile, and data variables are aligned along the independent dimension `time`.

File names in Level 1 are generally indicative of launch times; however for sondes that did not detect a launch, the file name indicates time of initialization. The attribute `Launch-time-(UTC)` in every sounding file of Level 2 should be considered as the final authority on launch time. This is the same as the variable *launch_time* in Levels 1 and 3.

`sonde_id` is a variable available in JOANNE products from Level 2 onwards. This is a unique, immutable identifier and is meant to identify exactly one dropsonde which corresponds to exactly one sounding profile. Note that the identifier variable `sounding_id` in the EUREC[4]A radiosonde dataset (Stephan et al., 2021) identifies sounding trajectory and not instrument, since one instrument can have upward and downward trajectories. The JOANNE variable `sonde_id` functions solely as an identifier, and no information should be interpreted from the semantics of this variable.

The Level-2 product consists of individual files for every sounding with the file structure as shown in Table 7. All files also include flight information such as position, height and speed as attributes. These are saved by the AVAPS aircraft computer in the sonde A files (see Table 4) and is input from the aircraft system itself. The files also have additional attributes such as the software version for post-processing and quality control. The file names are in the following format: `[campaign]_[project]_[instrument]_ [sonde_id]_[version].nc`, e.g., `EUREC4A_JOANNE_Dropsonde-RD41_HALO-0124_s42_v0.11.0.nc`. Note that `sonde_id` includes one underscore character within its value for the example shown.

5.2 Level 3 (gridded data)

Level 3 is a product combining dropsonde measurements launched from both the HALO and P3 aircraft, interpolated onto a uniform vertical grid of 10 m spacing, similar to the processing of EUREC[4]A radiosounding profiles (Stephan et al., 2021). The product is a single file which contains all dropsondes from Level 2 along the altitude dimension `alt`.

Table 7. Table shows the structure for the Level-2 product, outlining the coordinates and variables and their corresponding descriptions, units and dimensions.

Object	Name	Description	Units	Dimension
Coordinates	time	Time of recorded measurement	seconds since 2020-01-01	Time
	alt	Geopotential height	m	Time
	lat	Latitude	degree_north	Time
	long	Longitude	degree_east	Time
Variables	p	Atmospheric pressure	Pa	Time
	ta	Air temperature	K	Time
	rh	Relative humidity		Time
	wspd	Wind speed	$m\,s^{-1}$	Time
	wdir	Wind direction	degrees	Time
	sonde_id	Sonde identifier		

5.2.1 Gridding

The primary objective behind the Level-3 product is gridding all soundings on a common vertical grid, thus making it easier to use the soundings for different analyses. The vertical grid spacing for the dataset is kept at 10 m, up to an altitude of 10 km.

In the case of a regular drop, i.e., if there are no issues like a fast fall, or a failed parachute, the average descent rate of the dropsondes is $\sim 21\,m\,s^{-1}$ at 12 km altitude and $\sim 11\,m\,s^{-1}$ close to the surface. The PTU sensors have a measurement frequency of 2 Hz, while the GPS has a 4 Hz measurement frequency. This would translate to a vertical sampling of roughly 9–10 m at HALO's flight altitude and 5–6 m close to the surface for the PTU values and correspondingly finer vertical sampling for the GPS-based measurements. Hence the data are slightly coarsened, and only for PTU values in the upper to mid-troposphere do the interpolated values exceed the resolution of the measurements. The gridding is carried out through the following steps.

1. Variables `q` (specific humidity), `theta` (potential temperature), `u` (eastward wind) and `v` (northward wind) are computed and added to the dataset (for details, see Sect. 5.2.2).

2. All variables along the height coordinate in the dataset are averaged on 10 m bins up to 10 km altitude. In cases where no data are available in the altitude bin, a linear interpolation from neighboring measurements along the height dimension is used to estimate the value in the altitude bin, with the restraint that the neighboring measurements are not further apart than 50 m. If data are not available within 50 m of the desired height level, values at that height level are assigned `_FillValue`. While this still allows for a few missing values (~ 2–3 considering a fall speed of 15–20 m s^{-1}), it does not lead to substantial artificial information created by the smoothened interpolation between points relatively farther away.

3. Pressure values are interpolated logarithmically, and these values replace the linearly interpolated pressure values.

4. Temperature (T) and relative humidity (RH) are the originally measured properties by the dropsonde sensors. However, for interpolation q and θ are preferred, as these variables are conserved. After interpolation, T and RH are recomputed from the interpolated values of θ and q. The recomputed values for T and RH replace the previously interpolated T and RH variables from the sounding.

5. Wind speed and wind direction are computed from the interpolated values of u and v and added to the interpolated dataset.

5.2.2 Added variables

The complete list of variables, their units and their dimensions for Level 3 are provided in Table 8. The descriptions of variables added in Level 3 are as follows.

Launch time (`launch_time`)

Level-3 data are of the trajectory type with a single timestamp associated with each sounding, i.e., the launch time. This variable is the same as `launch_time` present in all Level-1 files.

Potential temperature θ (`theta`) and **specific humidity** q (`q`)

For estimating θ, we consider standard pressure, i.e., 1000 hPa. For the estimation of saturated vapor pressure, the method by Hardy (1998) is used with temperature at every altitude level as input, and subsequently, specific humidity (q) is estimated. The values of θ and q are estimated from the soundings on their respective raw vertical grid before interpolating them on to a common grid.

Platform name (`platform`)

Although all soundings are in a single file in Level 3, they can still be separated into HALO and P3 sondes, using this variable, which specifies the platform from which the dropsonde was launched. The values of the variable are strings and have two possible values – "HALO" and "P3".

Interpolated time (`interpolated_time`)

Since time is the independent dimension along which the measurements are made, it is illogical to average or interpolate time along the altitude dimension. Therefore, `time` is not available as a variable from Level 3 onwards. However, for practical purposes, this can be useful information, for instance, to compare with remote-sensing instruments on the aircraft. Thus, relying on the high sampling rate and based on the robust assumption that the dropsondes have negligible upward motion, Level 3 includes the variable `interpolated_time`. The variable is computed with linear interpolation, same as for other variables except pressure.

Low flight height flag (`low_height_flag`)

Some of the sondes from the P3 were launched at an altitude of ~ 3 km when the aircraft was also launching AXBTs. Therefore, these soundings sampled only the lower levels of the atmosphere, over just half of the depth sampled by other P3 sondes and a third of that of HALO's typical sondes. The `low_height_flag` variable in Level 3 marks sondes that have a launch altitude of less than 4 km, with a value of 1 and otherwise 0. This flag is useful to put in to context estimates of integrated quantities such as total column moisture, as well as to act as an easy separator for users who want to look at profiles in the free troposphere.

Number of measurements in bin (`N_p`, `N_ta`, `N_rh`, `N_gps` and bin method (`m_p`, `m_ta`, `m_rh`, `m_gps`))

The variables `N_p`, `N_ta`, `N_rh` and `N_gps` provide the number of pressure, temperature, relative humidity and GPS measurements, respectively, in each altitude bin for gridding. Depending on the values of these `N` variables, the corresponding cell methods – denoted by the `m` variables – are provided. For the `m` variables, possible values are 0, 1 and 2 and stand for no data, interpolation and averaging, respectively.

5.3   Level 4 (circle products)

As discussed in Sect. 2.2, the estimation of area-averaged mesoscale properties, such as divergence, was the primary objective behind the sondes' deployment over circular patterns. The Level-4 product provides these circle products as

gradient terms estimated by regressing the parameters at each level for a set of sondes comprising a circle. Level 4 also includes terms of divergence, vorticity, vertical velocity and pressure velocity, which are subsequently computed from the gradient terms. The input data are from the gridded dataset in Level 3.

5.3.1   Identifying circles and corresponding sondes

To aid in processing EUREC^{4}A data from aircraft, flight tracks for HALO and P3 were "segmented" into different standard categories such as circles and cloud modules. The flight phase segmentation (FPS) is described in more detail in Konow et al. (2021). We use these FPS files to identify the circles and the dropsondes corresponding to these circle segments. To facilitate ease of working with JOANNE and the FPS files, the circle segments in JOANNE Level 4 have been tagged with the same segment IDs as those in the FPS files. Moreover, the FPS files include a list of dropsondes associated with every flight segment, and this list is comprised of sonde IDs that are the same as that in the JOANNE Level-3 gridded product.

5.3.2   Regression

Following Bony and Stevens (2019), for any parameter ϕ measured by a dropsonde, assuming that variation at any altitude level is linear in horizontal space and is steady in time, the value at any point can be estimated as

$$\phi(x, y) \approx \phi_o + \frac{\partial \phi}{\partial x} \Delta x + \frac{\partial \phi}{\partial y} \Delta y, \tag{2}$$

where ϕ_o is the mesoscale mean value, and Δx and Δy are the eastward and northward distances, respectively, from the mean center point of all observed points included in the regression. Minimizing the least-squared errors for the linear regression fit shown in Eq. (2) would give an estimate of the linear variation in the eastward ($\frac{\partial \phi}{\partial x}$) and northward ($\frac{\partial \phi}{\partial y}$) directions, along with a value for the intercept for the line (ϕ_o), providing the mean mesoscale value for ϕ. Formulating this least-squares problem for an overdetermined system of k points as

$$\min_{x} \|\mathbf{A}\mathbf{x} - \mathbf{b}\|_2, \tag{3}$$

where $\mathbf{A} = \begin{pmatrix} 1 & \Delta x_1 & \Delta y_1 \\ 1 & \Delta x_2 & \Delta y_2 \\ \dots & \dots & \dots \\ 1 & \Delta x_k & \Delta y_k \end{pmatrix}$, $\mathbf{x} = \begin{pmatrix} \phi_o \\ \partial_x \phi \\ \partial_y \phi \end{pmatrix}$ and $\mathbf{b} =$

$\begin{pmatrix} \phi_1 \\ \phi_2 \\ \dots \\ \phi_k \end{pmatrix}$, we solve for $\mathbf{x}$ and compute the regression estimates as

$$\mathbf{x} = \mathbf{A}^+ \mathbf{b}, \tag{4}$$

Table 8. The structure for the Level-3 product, outlining the coordinates and variables and their corresponding descriptions, units and dimensions.

Object	Name	Description	Units	Dimension
Coordinates	alt	Height obtained by integrating the atmospheric thickness estimated from the hypsometric equation upwards	m	alt
	sonde_id	Unique sonde ID		sonde_id
	launch_time	Time of dropsonde launch	seconds since 2020-01-01	sonde_id
	interpolated_time	Value of time (original independent dimension) linearly interpolated to altitude grid	seconds since 2020-01-01	sonde_id, alt
	lat	Latitude	degree_north	sonde_id, alt
	long	Longitude	degree_east	sonde_id, alt
Variables	p	Atmospheric pressure	Pa	sonde_id, alt
	ta	Dry bulb temperature	K	sonde_id, alt
	rh	Relative humidity		sonde_id, alt
	wspd	Wind speed	$\mathrm{m\,s^{-1}}$	sonde_id, alt
	wdir	Wind direction	degree	sonde_id, alt
	u	u component of the wind	$\mathrm{m\,s^{-1}}$	sonde_id, alt
	v	v component of the wind	$\mathrm{m\,s^{-1}}$	sonde_id, alt
	theta	Air potential temperature	K	sonde_id, alt
	q	Specific humidity	$\mathrm{kg\,kg^{-1}}$	sonde_id, alt
	low_height_flag	Flag if flight height < 4 km when dropsonde was launched		sonde_id
	platform_id	Platform from which dropsonde was launched		sonde_id
	flight_altitude	Altitude of the aircraft when dropsonde was launched	m	sonde_id
	flight_lat	North latitude of the aircraft when dropsonde was launched	degree_north	sonde_id
	flight_lon	East longitude of the aircraft when dropsonde was launched	degree_east	sonde_id
	N_p	Number of observations used to derive Level-3 pressure data		sonde_id, alt
	N_ta	Number of observations used to derive Level-3 temperature data		sonde_id, alt
	N_rh	Number of observations used to derive Level-3 relative humidity data		sonde_id, alt
	N_gps	Number of observations used to derive Level-3 GPS data		sonde_id, alt
	m_p	Method used to derive Level-3 pressure data		sonde_id, alt
	m_ta	Method used to derive Level-3 temperature data		sonde_id, alt
	m_rh	Method used to derive Level-3 relative humidity data		sonde_id, alt
	m_gps	Method used to derive Level-3 GPS data		sonde_id, alt
	alt_bnds	Cell interval bounds for altitude	m	alt, nv

where $\mathbf{A}^+$ is the Moore–Penrose pseudo-inverse. This pseudo-inverse is obtained from the components of singular value decomposition (SVD) of $\mathbf{A}$. If the SVD of $\mathbf{A}$ is written as $U \cdot \Sigma \cdot V^T$, then $\mathbf{A}^+$ is estimated from the inverse of the SVD components as $V \cdot \Sigma^+ \cdot U^T$. Here, U and V are unitary matrices, Σ is a rectangular diagonal matrix with $\mathbf{A}$'s singular values and Σ^+ is a rectangular diagonal matrix with the reciprocal of $\mathbf{A}$'s singular values. We use the `linalg.pinv` function from the numpy Python library (v1.18.3) to calculate $\mathbf{A}^+$.

As a sanity check, we tested the Moore–Penrose pseudo-inverse method of least-squares fitting against the ordinary least-squares fitting by Bony and Stevens (2019), and we found no difference between the solutions (not shown). The advantage with incorporating SVD in the regression is that it significantly reduces computing time, because of the availability of vectorized functions in the numpy library.

The Level-4 product includes the eastward (zonal) and northward (meridional) gradients of temperature, pressure, specific humidity, and u and v winds. Derived from these, Level 4 also provides area-averaged mesoscale divergence ($\mathcal{D}$), vorticity (ζ), vertical velocity (W) and pressure velocity (ω), following Bony and Stevens (2019). The dataset also provides the standard error of each of these regressed estimates as ancillaries to the corresponding variables, thus establishing an extent of confidence in the calculation of these mesoscale properties.

Derived variables in Level 4 are at the same vertical grid of 10 m spacing as in Level 3, and the number of sondes regressed at every level is provided as a variable (`sondes_regressed`). If at any level, fewer than six sondes have data available, the value for regressed values at that level is set to not a number (NaN). This includes data missing due to no data being recorded as well as sondes removed in any of the previous QC steps. Since the number of sondes regressed change at different levels, this causes abrupt, but generally minor, fluctuations in integrated products such as pressure velocity and vertical velocity.

All data variables in Level 4 are along the `circle` and `alt` dimensions (see Table 9), and individual sounding data are excluded. The list of sonde IDs included in every circle is included as a variable along dimension `sonde_id`, making it easier to retrieve data for the individual soundings in the circle.

6 Code and data availability

The JOANNE dataset described in this paper is freely available at AERIS (https://doi.org/10.25326/246, George et al., 2021b). The software used to process the dropsonde data and create JOANNE is also publicly available (https://doi.org/10.5281/zenodo.4746312, George, 2021).

7 Summary

The EUREC⁴A field campaign took place in January–February 2020 over the North Atlantic trade-wind region. The campaign employed a multitude of platforms measuring a range of atmospheric and oceanographic variables with the objective of understanding shallow clouds and processes that influence them. A core part of the campaign was the deployment of dropsondes to characterize the thermodynamic and dynamic structure of the atmospheric environment. Here, we present JOANNE, the dataset that provides these dropsonde data and additional derived products.

JOANNE presents measurements from 1215 dropsondes launched during EUREC⁴A by the German research aircraft HALO and the NOAA WP-3D. Dropsondes were primarily released in groups of 12, circumscribing a mesoscale ~ 222 km diameter circle centered near 13.3° N, 57.7° W, which we call the EUREC⁴A-circle. A total of 85 circle patterns were flown with dropsonde launches, 73 being flown by HALO over the EUREC⁴A-circle along patterns that were not biased toward particular meteorological conditions. In addition, sondes were launched on circular flight patterns centered elsewhere, along lawn-mower flight patterns coinciding with AXBT drops and in a variety of other locations to provide context or calibration for other measurements. Data presented in JOANNE have been quality controlled to eliminate sondes with no, or partially corrupted, data. A total of 51 of the 1215 sondes did not provide usable data, and another 98 provided only partial data and are not included in data products from Level 2 onwards.

A comparison of the HALO dropsondes with radiosondes intensively launched from the R/V *Meteor* close to the western (upwind) edge of the EUREC⁴A-circle and with radiosondes launched from the downwind Barbados Cloud Observatory suggests a dry bias. Multiplying relative humidity values by 1.06 appears to largely correct the bias and therefore has been applied from Level 2 onwards to relative humidity and variables derived from it. We found no evidence of such a bias in the P3 sondes, and the reason for the dry bias in HALO seems attributable to a lack of reconditioning of the HALO sondes.

JOANNE is divided into five levels of data products, with increasing order of processing and product retrieval. Level 0 comprises the raw measurement data from the dropsondes collected by AVAPS on the aircraft. Level 1 provides data processed using ASPEN – a state-of-the-art tool for processing raw dropsonde data files. Level 2 consists of individual sounding files that passed through the QC check, but with redundant quantities removed and no derived variables added. Level 3 provides the data after gridding them to a uniform vertical spacing of 10 m, along with derived variables such as potential temperature and specific humidity. Level 4 contains the circle products which are area-averaged and mesoscale variables such as gradients, divergence, vorticity and vertical velocity. Possible sources of uncertainty in JOANNE include

Table 9. The structure for the Level-4 product, outlining the coordinates and variables and their corresponding descriptions, units and dimensions. The ancillary variables (with the prefix "se_") give the standard error for their corresponding variables indicated by the suffix in the name.

Object	Name	Description	Units	Dimension
Coordinates	alt	Height obtained by integrating upwards the atmospheric thickness estimated from the hypsometric equation	m	alt
	sounding	Sonde number		sounding
	circle	Circle number		circle
	circle_lon	Longitude of fitted circle for all regressed sondes in circle	degree_east	circle
	circle_lat	Latitude of fitted circle for all regressed sondes in circle	degree_north	circle
	circle_time	Mean launch time of all sondes in circle	seconds since 2020-01-01	circle
	segment_id	Unique segment ID		circle
Variables	platform_id	Platform which flew the circle		circle
	flight_altitude	Mean altitude of the aircraft during the circle	m	circle
	circle_diameter	Diameter of fitted circle for all regressed sondes in circle	m	circle
	u	Mean eastward wind in circle	$m\,s^{-1}$	circle, alt
	dudx	Zonal gradient of eastward wind	s^{-1}	circle, alt
	dudy	Meridional gradient of eastward wind	s^{-1}	circle, alt
	sonde_id	Unique sonde ID		circle, sounding
	v	Mean northward wind in circle	$m\,s^{-1}$	circle, alt
	dvdx	Zonal gradient of northward wind	s^{-1}	circle, alt
	dvdy	Meridional gradient of northward wind	s^{-1}	circle, alt
	q	Mean specific humidity in circle	$kg\,kg^{-1}$	circle, alt
	dqdx	Zonal gradient of specific humidity	$kg\,kg^{-1}\,m^{-1}$	circle, alt
	dqdy	Meridional gradient of specific humidity	$kg\,kg^{-1}\,m^{-1}$	circle, alt
	ta	Mean air temperature in circle	K	circle, alt
	dtadx	Zonal gradient of temperature	$K\,m^{-1}$	circle, alt
	dtady	Meridional gradient of temperature	$K\,m^{-1}$	circle, alt
	p	Mean air pressure in circle	Pa	circle, alt
	dpdx	Zonal gradient of pressure	$Pa\,m^{-1}$	circle, alt
	dpdy	Meridional gradient of pressure	$Pa\,m^{-1}$	circle, alt
	D	Area-averaged horizontal mass divergence	s^{-1}	circle, alt
	vor	Area-averaged horizontal relative vorticity	s^{-1}	circle, alt
	W	Area-averaged vertical air velocity	$m\,s^{-1}$	circle, alt
	se_dudx		s^{-1}	circle, alt
	se_dudy		s^{-1}	circle, alt

Table 9. Continued.

Object	Name	Description	Units	Dimension
	se_dvdx		s^{-1}	circle, alt
	se_dvdy		s^{-1}	circle, alt
	se_dqdx		$kg\,kg^{-1}\,m^{-1}$	circle, alt
	se_dqdy		$kg\,kg^{-1}\,m^{-1}$	circle, alt
	se_dpdx		$Pa\,m^{-1}$	circle, alt
	se_dpdy		$Pa\,m^{-1}$	circle, alt
	se_dtadx		$K\,m^{-1}$	circle, alt
	se_dtady		$K\,m^{-1}$	circle, alt
	se_D		s^{-1}	circle, alt
	se_vor		s^{-1}	circle, alt
	se_W		$m\,s^{-1}$	circle, alt
	omega	Area-averaged atmospheric pressure velocity	$Pa\,s^{-1}$	circle, alt
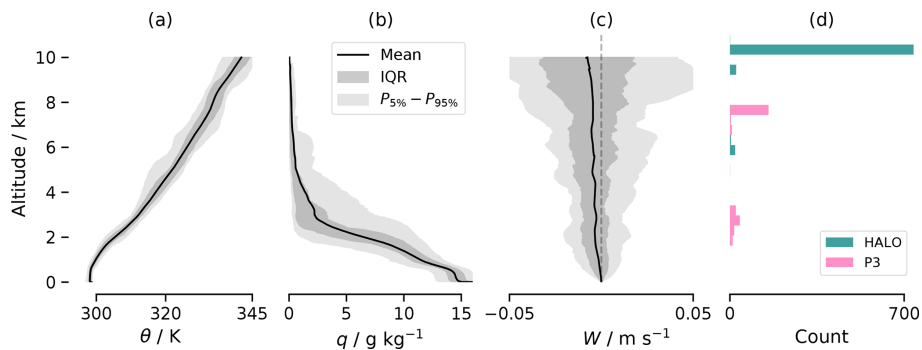
Figure 6. Vertical profiles of mean potential temperature **(a)** and specific humidity **(b)** from measurements of HALO and P3 sondes. Panel **(c)** shows the vertical profile of mean vertical velocity from estimates of HALO's EUREC^{4}A-circle measurements. Darkly and lightly shaded regions in **(a)**–**(c)** show inter-quartile range (IQR) and 5th–95th percentile range, respectively. Panel **(d)** shows the histogram for the flight altitude of dropsondes launched from both platforms.

sensors' repeatability of measurements (see Table 1), uncertainty from the correction of dry bias in HALO sondes (see Sect. 4) and errors arising from the regression estimates (see Sect. 5.3.2).

JOANNE's immediate usefulness lies in aiding the calibration of or processing the data from remote-sensing instruments on board HALO as well as creation of derived products, e.g., a dataset of radiative profiles from EUREC^{4}A soundings (Albright et al., 2021). Furthermore, the dataset potentially has applications in furthering the understanding of processes in the trades, e.g., the influence of mesoscale circulation on clouds (George et al., 2021a) or the changes in atmospheric properties within a cold pool (Touzé-Peiffer et al., 2021). The vertical profiles and histogram of flight altitude for dropsonde launches shown in Fig. 6 provide an overview for a subset of the atmospheric observations that JOANNE

provides. While reaffirming the typical steadiness in the thermodynamic structure of the trades, JOANNE also confirms the high variability in mesoscale vertical motion found by Bony and Stevens (2019) compared to the mean over longer timescales.

Author contributions. JOANNE was conceived by GG. BS and SB designed the sounding strategy for EUREC^{4}A, and RP and CF adapted this for the P3's participation through ATOMIC. HS and TK contributed to the design and processing of the data. GG and BS performed the quality control. The manuscript was mainly written by GG with contributions by BS. GG, HS, MK, HK, MP and JR were responsible for dropsonde launch operations and real-time data quality control over different HALO flights. QTK and AL were

responsible for processing and quality-controlling the data for the P3 flights. All authors read and approved the manuscript.

Disclaimer. Publisher's note: Copernicus Publications remains neutral with regard to jurisdictional claims in published maps and institutional affiliations.

Special issue statement. This article is part of the special issue "Elucidating the role of clouds–circulation coupling in climate: datasets from the 2020 (EUREC^{4}A) field campaign". It is not associated with a conference.

Review statement. This paper was edited by Silke Gross and reviewed by two anonymous referees.

References

Albright, A. L., Fildier, B., Touzé-Peiffer, L., Pincus, R., Vial, J., and Muller, C.: Atmospheric radiative profiles during EUREC^{4}A, Earth Syst. Sci. Data, 13, 617–630, https://doi.org/10.5194/essd-13-617-2021, 2021.

Bony, S. and Stevens, B.: Measuring Area-Averaged Vertical Motions with Dropsondes, J. Atmos. Sci., 76, 767–783, https://doi.org/10.1175/JAS-D-18-0141.1, 2019.

Bony, S., Stevens, B., Ament, F., Bigorre, S., Chazette, P., Crewell, S., Delanoë, J., Emanuel, K., Farrell, D., Flamant, C., Gross, S., Hirsch, L., Karstensen, J., Mayer, B., Nuijens, L., Ruppert, J. H., Sandu, I., Siebesma, P., Speich, S., Szczap, F., Totems, J., Vogel, R., Wendisch, M., and Wirth, M.: EUREC^{4}A: A field campaign to elucidate the couplings between clouds, convection and circulation, Surv. Geophys., 38, 1–40, https://doi.org/10.1007/s10712-017-9428-0, 2017.

Fleming, J. R.: First woman: Joanne Simpson and the tropical atmosphere, Oxford University Press, https://doi.org/10.1093/oso/9780198862734.001.0001, 2020.

George, G.: JOANNE (Joint dropsonde Observations of the Atmosphere in tropical North atlaNtic meso-scale Environments) software, Zenodo [code], https://doi.org/10.5281/zenodo.4746312, 2021.

George, G., Stevens, B., Bony, S., Klingebiel, M., and Vogel, R.: Observed impact of meso-scale vertical motion on cloudiness, J. Atmos. Sci., 78, 2413–2427, https://doi.org/10.1175/JAS-D-20-0335.1, 2021a.

George, G., Stevens, B., Bony, S., Pincus, R., Fairall, C., Schulz, H., Kölling, T., Kalen, Q. T., Klingebiel, M., Konow, H., Lundry, A., Prange, M., and Radtke, J.: JOANNE: Joint dropsonde Observations of the Atmosphere in tropical North atlaNtic meso-scale Environments (v2.0.0), AERIS [data set], https://doi.org/10.25326/246, 2021b.

Hardy, B.: ITS-90 Formulations for Vapor Pressure, Frostpoint Temperature, Dewpoint Temperature, and Enhancement Factors in the Range -100 to $+100$ C, Proceedings of the Third International Symposium on Humidity and Moisture, April 1998, Teddington, London, UK, 1998.

Konow, H., Jacob, M., Ament, F., Crewell, S., Ewald, F., Hagen, M., Hirsch, L., Jansen, F., Mech, M., and Stevens, B.: A unified data set of airborne cloud remote sensing using the HALO Microwave Package (HAMP), Earth Syst. Sci. Data, 11, 921–934, https://doi.org/10.5194/essd-11-921-2019, 2019.

Konow, H., Ewald, F., George, G., Jacob, M., Klingebiel, M., Kölling, T., Luebke, A. E., Mieslinger, T., Pörtge, V., Radtke, J., Schäfer, M., Schulz, H., Vogel, R., Wirth, M., Bony, S., Crewell, S., Ehrlich, A., Forster, L., Giez, A., Gödde, F., Groß, S., Gutleben, M., Hagen, M., Hirsch, L., Jansen, F., Lang, T., Mayer, B., Mech, M., Prange, M., Schnitt, S., Vial, J., Walbröl, A., Wendisch, M., Wolf, K., Zinner, T., Zöger, M., Ament, F., and Stevens, B.: EUREC^{4}A's HALO, Earth Syst. Sci. Data Discuss. [preprint], https://doi.org/10.5194/essd-2021-193, in review, 2021.

Lenschow, D. H., Krummel, P. B., and Siems, S. T.: Measuring Entrainment, Divergence, and Vorticity on the Mesoscale from Aircraft, J. Atmos. Ocean. Tech., 16, 1384–1400, https://doi.org/10.1175/1520-0426(1999)016<1384:MEDAVO>2.0.CO;2, 1999.

Lenschow, D. H., Savic-Jovcic, V., and Stevens, B.: Divergence and Vorticity from Aircraft Air Motion Measurements, J. Atmos. Ocean. Tech., 24, 2062–2072, https://doi.org/10.1175/2007JTECHA940.1, 2007.

Martin, C. and Suhr, I.: NCAR/EOL Atmospheric Sounding Processing ENvironment (ASPEN) software, Version 3.4.3, available at: https://www.eol.ucar.edu/content/aspen, last access: 9 November 2021.

Pincus, R., Fairall, C. W., Bailey, A., Chen, H., Chuang, P. Y., de Boer, G., Feingold, G., Henze, D., Kalen, Q. T., Kazil, J., Leandro, M., Lundry, A., Moran, K., Naeher, D. A., Noone, D., Patel, A. J., Pezoa, S., PopStefanija, I., Thompson, E. J., Warnecke, J., and Zuidema, P.: Observations from the NOAA P-3 aircraft during ATOMIC, Earth Syst. Sci. Data, 13, 3281–3296, https://doi.org/10.5194/essd-13-3281-2021, 2021.

Stephan, C. C., Schnitt, S., Schulz, H., Bellenger, H., de Szoeke, S. P., Acquistapace, C., Baier, K., Dauhut, T., Laxenaire, R., Morfa-Avalos, Y., Person, R., Quiñones Meléndez, E., Bagheri, G., Böck, T., Daley, A., Güttler, J., Helfer, K. C., Los, S. A., Neuberger, A., Röttenbacher, J., Raeke, A., Ringel, M., Ritschel, M., Sadoulet, P., Schirmacher, I., Stolla, M. K., Wright, E., Charpentier, B., Doerenbecher, A., Wilson, R., Jansen, F., Kinne, S., Reverdin, G., Speich, S., Bony, S., and Stevens, B.: Ship- and island-based atmospheric soundings from the 2020 EUREC⁴A field campaign, Earth Syst. Sci. Data, 13, 491–514, https://doi.org/10.5194/essd-13-491-2021, 2021.

Stevens, B., Farrell, D., Hirsch, L., Jansen, F., Nuijens, L., Serikov, I., Brügmann, B., Forde, M., Linne, H., Lonitz, K., and Prospero, J. M.: The barbados cloud observatory: anchoring investigations of clouds and circulation on the edge of the ITCZ, B. Am. Meteorol. Soc., 97, 787–801, https://doi.org/10.1175/BAMS-D-14-00247.1, 2016.

Stevens, B., Brogniez, H., Kiemle, C., Lacour, J.-L., Crevoisier, C., and Kiliani, J.: Structure and dynamical influence of water vapor in the lower tropical troposphere, Surv. Geophys., 38, 1–27, https://doi.org/10.1007/s10712-017-9420-8, 2017.

Stevens, B., Bony, S., Farrell, D., Ament, F., Blyth, A., Fairall, C., Karstensen, J., Quinn, P. K., Speich, S., Acquistapace, C., Aemisegger, F., Albright, A. L., Bellenger, H., Bodenschatz, E., Caesar, K.-A., Chewitt-Lucas, R., de Boer, G., Delanoë, J., Denby, L., Ewald, F., Fildier, B., Forde, M., George, G., Gross, S., Hagen, M., Hausold, A., Heywood, K. J., Hirsch, L., Jacob, M., Jansen, F., Kinne, S., Klocke, D., Kölling, T., Konow, H., Lothon, M., Mohr, W., Naumann, A. K., Nuijens, L., Olivier, L., Pincus, R., Pöhlker, M., Reverdin, G., Roberts, G., Schnitt, S., Schulz, H., Siebesma, A. P., Stephan, C. C., Sullivan, P., Touzé-Peiffer, L., Vial, J., Vogel, R., Zuidema, P., Alexander, N., Alves, L., Arixi, S., Asmath, H., Bagheri, G., Baier, K., Bailey, A., Baranowski, D., Baron, A., Barrau, S., Barrett, P. A., Batier, F., Behrendt, A., Bendinger, A., Beucher, F., Bigorre, S., Blades, E., Blossey, P., Bock, O., Böing, S., Bosser, P., Bourras, D., Bouruet-Aubertot, P., Bower, K., Branellec, P., Branger, H., Brennek, M., Brewer, A., Brilouet , P.-E., Brügmann, B., Buehler, S. A., Burke, E., Burton, R., Calmer, R., Canonici, J.-C., Carton, X., Cato Jr., G., Charles, J. A., Chazette, P., Chen, Y., Chilinski, M. T., Choularton, T., Chuang, P., Clarke, S., Coe, H., Cornet, C., Coutris, P., Couvreux, F., Crewell, S., Cronin, T., Cui, Z., Cuypers, Y., Daley, A., Damerell, G. M., Dauhut, T., Deneke, H., Desbios, J.-P., Dörner, S., Donner, S., Douet, V., Drushka, K.,

Dütsch, M., Ehrlich, A., Emanuel, K., Emmanouilidis, A., Etienne, J.-C., Etienne-Leblanc, S., Faure, G., Feingold, G., Ferrero, L., Fix, A., Flamant, C., Flatau, P. J., Foltz, G. R., Forster, L., Furtuna, I., Gadian, A., Galewsky, J., Gallagher, M., Gallimore, P., Gaston, C., Gentemann, C., Geyskens, N., Giez, A., Gollop, J., Gouirand, I., Gourbeyre, C., de Graaf, D., de Groot, G. E., Grosz, R., Güttler, J., Gutleben, M., Hall, K., Harris, G., Helfer, K. C., Henze, D., Herbert, C., Holanda, B., Ibanez-Landeta, A., Intrieri, J., Iyer, S., Julien, F., Kalesse, H., Kazil, J., Kellman, A., Kidane, A. T., Kirchner, U., Klingebiel, M., Körner, M., Kremper, L. A., Kretzschmar, J., Krüger, O., Kumala, W., Kurz, A., L'Hégaret, P., Labaste, M., Lachlan-Cope, T., Laing, A., Landschützer, P., Lang, T., Lange, D., Lange, I., Laplace, C., Lavik, G., Laxenaire, R., Le Bihan, C., Leandro, M., Lefevre, N., Lena, M., Lenschow, D., Li, Q., Lloyd, G., Los, S., Losi, N., Lovell, O., Luneau, C., Makuch, P., Malinowski, S., Manta, G., Marinou, E., Marsden, N., Masson, S., Maury, N., Mayer, B., Mayers-Als, M., Mazel, C., McGeary, W., McWilliams, J. C., Mech, M., Mehlmann, M., Meroni, A. N., Mieslinger, T., Minikin, A., Minnett, P., Möller, G., Morfa Avalos, Y., Muller, C., Musat, I., Napoli, A., Neuberger, A., Noisel, C., Noone, D., Nordsiek, F., Nowak, J. L., Oswald, L., Parker, D. J., Peck, C., Person, R., Philippi, M., Plueddemann, A., Pöhlker, C., Pörtge, V., Pöschl, U., Pologne, L., Posyniak, M., Prange, M., Quiñones Meléndez, E., Radtke, J., Ramage, K., Reimann, J., Renault, L., Reus, K., Reyes, A., Ribbe, J., Ringel, M., Ritschel, M., Rocha, C. B., Rochetin, N., Röttenbacher, J., Rollo, C., Royer, H., Sadoulet, P., Saffin, L., Sandiford, S., Sandu, I., Schäfer, M., Schemann, V., Schirmacher, I., Schlenczek, O., Schmidt, J., Schröder, M., Schwarzenboeck, A., Sealy, A., Senff, C. J., Serikov, I., Shohan, S., Siddle, E., Smirnov, A., Späth, F., Spooner, B., Stolla, M. K., Szkółka, W., de Szoeke, S. P., Tarot, S., Tetoni, E., Thompson, E., Thomson, J., Tomassini, L., Totems, J., Ubele, A. A., Villiger, L., von Arx, J., Wagner, T., Walther, A., Webber, B., Wendisch, M., Whitehall, S., Wiltshire, A., Wing, A. A., Wirth, M., Wiskandt, J., Wolf, K., Worbes, L., Wright, E., Wulfmeyer, V., Young, S., Zhang, C., Zhang, D., Ziemen, F., Zinner, T., and Zöger, M.: EUREC⁴A, Earth Syst. Sci. Data, 13, 4067–4119, https://doi.org/10.5194/essd-13-4067-2021, 2021.

Touzé-Peiffer, L., Vogel, R., and Rochetin, N.: Detecting cold pools from soundings during EUREC⁴A, EGU General Assembly 2021, online, 19–30 April 2021, EGU21-1038, https://doi.org/10.5194/egusphere-egu21-1038, 2021.

UCAR/NCAR – Earth Observing Laboratory: NCAR Airborne Vertical Atmospheric Profiling System (AVAPS), UCAR/NCAR – Earth Observing Laboratory, https://doi.org/10.5065/d66w9848, 1993.

Vaisala: Vaisala Radiosonde RD41 datasheet in English, B211706EN-B, Tech. rep., Vaisala, available at: https://www.vaisala.com/sites/default/files/documents/RD41-Datasheet-B211706EN.pdf (last access: 9 November 2021), 2020a.

Vaisala: Vaisala Radiosonde RS41G datasheet in English, B211321EN-K, Tech. rep., Vaisala, available at: https://www.vaisala.com/sites/default/files/documents/RS41-SG-Datasheet-B211321EN.pdf (last access: 9 November 2021), 2020b.

Vömel, H., Goodstein, M., Tudor, L., Witte, J., Fuchs-Stone, Ž., Sentić, S., Raymond, D., Martinez-Claros, J., Juračić, A.,

Maithel, V., and Whitaker, J. W.: High-resolution in situ observations of atmospheric thermodynamics using dropsondes during the Organization of Tropical East Pacific Convection (OTREC) field campaign, Earth Syst. Sci. Data, 13, 1107–1117, https://doi.org/10.5194/essd-13-1107-2021, 2021.